Cell

Structural Linkage between Ligand Discrimination and Receptor Activation by Type I Interferons

Christoph Thomas,[1] Ignacio Moraga,[1] Doron Levin,[4] Peter O. Krutzik,[2] Yulia Podoplelova,[5] Angelica Trejo,[2] Choongho Lee,[3] Ganit Yarden,[4] Susan E. Vleck,[3] Jeffrey S. Glenn,[3] Garry P. Nolan,[2] Jacob Piehler,[5] Gideon Schreiber,[4] and K. Christopher Garcia[1,*]

[1]Howard Hughes Medical Institute, Department of Molecular and Cellular Physiology and Department of Structural Biology
[2]Department of Microbiology and Immunology, Baxter Lab in Stem Cell Biology
[3]Department of Medicine, Division of Gastroenterology and Hepatology
Stanford University School of Medicine, Stanford, CA 94305, USA
[4]Department of Biological Chemistry, Weizmann Institute of Science, Rehovot 76100, Israel
[5]Division of Biophysics, University of Osnabrück, 49076 Osnabrück, Germany
*Correspondence: kcgarcia@stanford.edu
DOI 10.1016/j.cell.2011.06.048

SUMMARY

Type I Interferons (IFNs) are important cytokines for innate immunity against viruses and cancer. Sixteen human type I IFN variants signal through the same cell-surface receptors, IFNAR1 and IFNAR2, yet they can evoke markedly different physiological effects. The crystal structures of two human type I IFN ternary signaling complexes containing IFNα2 and IFNω reveal recognition modes and heterotrimeric architectures that are unique among the cytokine receptor superfamily but conserved between different type I IFNs. Receptor-ligand cross-reactivity is enabled by conserved receptor-ligand "anchor points" interspersed among ligand-specific interactions that "tune" the relative IFN-binding affinities, in an apparent extracellular "ligand proofreading" mechanism that modulates biological activity. Functional differences between IFNs are linked to their respective receptor recognition chemistries, in concert with a ligand-induced conformational change in IFNAR1, that collectively control signal initiation and complex stability, ultimately regulating differential STAT phosphorylation profiles, receptor internalization rates, and downstream gene expression patterns.

INTRODUCTION

IFNs were the first cytokines discovered more than half a century ago as agents that interfere with viral infection (Borden et al., 2007; Isaacs and Lindenmann, 1957). IFNs have been established as pleiotropic, multifunctional proteins in the early immune response, exhibiting antiproliferative effects on cells, in addition to their strong immunomodulatory and antiviral activities. Due to their potency and diverse biological activities, IFNs are used for the treatment of several human diseases, including hepatitis C, multiple sclerosis, and certain types of cancer (Borden et al., 2007). Based on the receptor system that mediates their effects, IFNs are grouped into type I, type II, and type III IFNs (Uzé et al., 2007). The type I IFNs act on, and are produced by, almost every nucleated cell and comprise 16 members with approximately 20%–60% sequence identity: IFNβ, IFNε, IFNκ, IFNω, and 12 subtypes of IFNα. IFNα, IFNβ, and IFNω are produced by cells exposed to viruses or double-stranded RNA (García-Sastre and Biron, 2006) and have been shown to possess antitumor activity (Horton et al., 1999; Pestka et al., 2004) as well as protect cells against parasites and bacterial pathogens (Bogdan, 2000). Although similar in their spectrum of activities, IFNβ, IFNω, and IFNα subtypes can vary significantly in their potency against different viruses, their antiproliferative activity, and their ability to activate cells of the immune system. The mechanism mediating this differential activity and signaling through a common receptor remains controversial (van Boxel-Dezaire et al., 2006).

Despite their differential activities and broad range of potencies, all 16 human type I IFNs initiate signaling by binding to the same receptor composed of two subunits called IFNAR1 and IFNAR2. Together with the IL-10 family receptors, the IL-20 receptor, IL-22R, IL-22BP, IFNLR1, tissue factor, and IFNGR, IFNAR1 and IFNAR2 form the class II helical cytokine receptor family (Pestka et al., 2004; Walter, 2004; Zdanov, 2010). In common with other class II helical cytokine receptors, the extracellular domain (ECD) of IFNAR2, whose nuclear magnetic resonance (NMR) structure has been characterized (Chill et al., 2003), consists of two fibronectin III (FNIII)-like domains (D1 and D2). The ECD of IFNAR1, however, is unique, comprising a tandem array of four FNIII subdomains, designated SD1 to SD4, which arose from gene duplication of the typical two-domain structure (Gaboriaud et al., 1990).

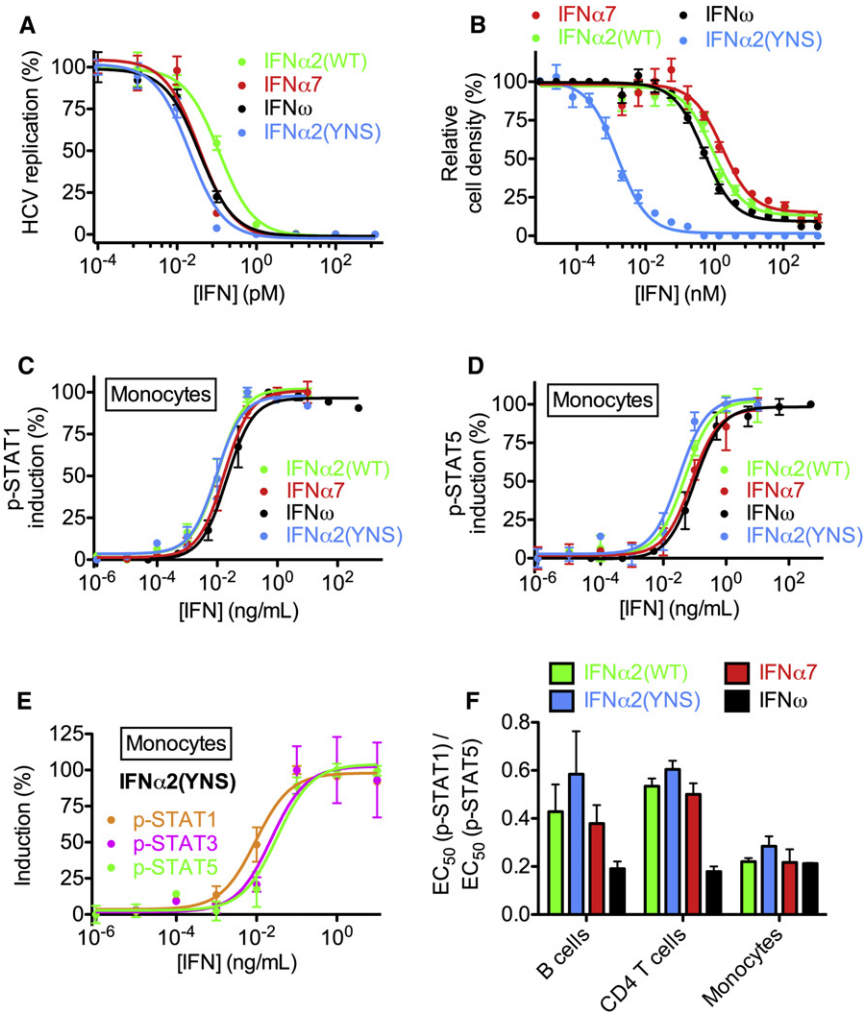

Figure 1. Differential Activities and Potencies of Type I IFNs

(A) Antiviral dose-response curves of human hepatoma (Huh7.5) cells transfected with genomic hepatitis C virus (HCV) RNA and treated with IFNα2(WT), IFNα2(YNS), IFNω, or IFNα7. Shown are mean values with their standard deviation.

(B) Antiproliferative dose-response curves of human amniotic epithelial (WISH) cells treated with IFNα2(WT), IFNα2(YNS), IFNω, or IFNα7. Shown are mean values with their standard error.

(C) Dose-response curves for STAT1 phosphorylation in monocytes from human whole blood, as determined by phospho-flow analysis. Shown are mean values with their standard error.

(D) Dose-response curves for STAT5 phosphorylation in monocytes from human whole blood, as determined by phospho-flow cytometry analysis. Shown are mean values with their standard error.

(E) IFNα2(YNS) more potently induces p-STAT1 than p-STAT3 or p-STAT5 in human primary monocytes. Shown are mean values with their standard error.

(F) Differential signaling properties of IFNα2(WT), IFNα2(YNS), IFNω, and IFNα7 as evidenced by different ratios of p-STAT1 to p-STAT5 EC_{50} values in different cell types from human whole blood. Shown are mean values with their standard error.

See also Figure S1.

The intracellular domains (ICDs) of IFNAR1 and IFNAR2 are associated with the Janus kinases (Jaks) Tyk2 and Jak1, respectively (Schindler and Plumlee, 2008; van Boxel-Dezaire et al., 2006). Upon ligand binding by the IFNAR chains and formation of the extracellular signaling complex, these tyrosine kinases initiate a phosphorylation cascade principally mediated by STAT (signal transducer and activator of transcription) activation (Schindler and Plumlee, 2008). Other important signaling pathways activated by type I IFNs include the phosphatidylinositol 3-kinase pathway and the MAP kinase pathway. Studies of the overlapping, yet differential cellular responses elicited by different members of the type I IFNs (Uzé et al., 2007) have suggested that the dynamics of ligand interaction with the receptor subunits plays a key role for regulating cellular response patterns (Jaitin et al., 2006; Jaks et al., 2007; Kalie et al., 2007).

There are currently no crystal structures of type I IFN receptor complexes nor any complete receptor signaling complex in the class II helical cytokine family where structures of binary complexes of ligands (IFNγ, IL-10, IL-22, IFNλ) with their high-affinity receptor subunits are known (Bleicher et al., 2008; Jones et al., 2008; Josephson et al., 2001; Miknis et al., 2010; Walter et al., 1995). Here we present structural and functional data that shed light on how type I IFNs engage their receptor chains, how the receptor system is able to recognize the large number of different ligands, and how the different chemistries of ligand interaction ultimately dictate the stabilities of the receptor complexes and therefore exert primary control on differential signaling.

RESULTS

Type I IFNs Exhibit Distinct Signaling and Functional Activities

We studied IFNs that differed significantly in their biological activities: IFNω, IFNα2, and a mutant of IFNα2, IFNα2(YNS), that was engineered to have higher affinity for IFNAR1 in order to improve its antitumor efficacy (Kalie et al., 2007). We tested their relative antiviral and antiproliferative potencies, as well as another type I IFN, IFNα7 (Figures 1A and 1B and Figure S5 available online). The half-maximal effective concentration (EC_{50}) values in a hepatitis C replication assay showed 2- to 6-fold differences between the IFNs (IFNα7: 36 fM, IFNω: 37 fM, IFNα2(YNS): 20 fM, wild-type (WT) IFNα2: 116 fM) (Figure 1A), whereas the antiproliferative activities on WISH cells differed by more than 1000-fold (EC_{50} values: IFNα7: 1700 pM, IFNω: 490 pM, IFNα2(YNS): 1.5 pM, IFNα2(WT): 890 pM) (Figure 1B).

We used phospho-flow cytometry coupled with fluorescent cell barcoding to compare the intracellular signaling activities of these IFNs by measuring phosphorylation of STATs in primary cells in whole blood from human donors (Krutzik and Nolan, 2006). This approach enabled us to measure IFN responses on endogenous IFN receptors of multiple cell subsets (B cells, monocytes, and CD8 and CD4 T cells) simultaneously without cell separation (Figures 1C–1F, Figure S1, and Figure S7). Although the potency of the different IFNs in inducing phosphorylation of STAT1 and STAT5 in monocytes is similar (Figures 1C and 1D), IFNα2(YNS) has a lower EC_{50} for p-STAT1 induction versus p-STAT3 and p-STAT5 (Figure 1E). Comparing the ratios of EC_{50}(p-STAT1) versus EC_{50}(p-STAT5) reveals that the different IFNs exhibit significant variability in different cell subsets (Figure 1F), with IFNα2(YNS) displaying the highest ratio of p-STAT1:p-STAT5 EC_{50} values in B cells, CD4 T cells, and monocytes, and IFNω producing the lowest ratio in all three cell subsets. Collectively, the cellular and signaling results highlight the puzzling properties of differential signaling through the common IFNAR1-IFNAR2 heterodimeric receptor.

The Architecture of the IFN Ternary Signaling Complex

We determined crystal structures of a range of individual IFN receptor components, a subcomplex, and ternary complexes at various resolutions (Figure 2 and Table S1): (1) the structure of unliganded IFNAR1 comprising SD1 through SD3 (IFNAR1ΔSD4) at 1.9 Å (Figure 2A); (2) the IFNAR2-D2 domain at 2.6 Å (Figure 2B); (3) the binary complex between IFNAR2 and IFNα2(HEQ) at 2.0 Å (Figure 2C); (4) the ternary ligand-receptor complex of IFNα2(YNS) (hereafter also referred to as IFNα2) at 4.0 Å (Figure 2D); (5) the ternary ligand-receptor complex of wild-type IFNω at 3.5 Å (Figure 2E). IFNα2(YNS) is a triple mutant (His57Tyr, Glu58Asn, Gln61Ser) of IFNα2 with high affinity for IFNAR1, and HEQ is the triple mutant to alanine (Jaitin et al., 2006). High-resolution structures of subcomponents determined here, and previously (IFNα2 and IFNAR2-D1 domain) (Quadt-Akabayov et al., 2006; Radhakrishnan et al., 1996), were used to solve the ternary complexes. Despite their lower resolution, the electron density maps of the ternary complexes (Figure S2) allowed refinement of almost all amino acids and clear visualization of conformational changes between the free and bound states (details in Extended Experimental Procedures). The SD4 of IFNAR1 has been shown to be unnecessary for IFN binding (Lamken et al., 2005) and, consistent with electron-microscopic studies (Li et al., 2008), it was not visible in the electron density maps. All structures can be viewed interactively at (http://proteopedia.org/w/Journal:Cell:1).

IFNAR1 and IFNAR2 bind on opposing sides of the IFN ligands in a nearly orthogonal architecture that has not been seen previously in crystal structures of cytokine-receptor complexes (Figures 2D and 2E). Both the IFNα2 and IFNω complexes exhibit almost identical overall receptor-ligand docking modes when the two ternary complexes are superimposed (root-mean-square deviation [rmsd] of Cα = 0.9 Å) (Figure 3A). The IFNAR1-IFN docking mode seen here is unusual and so far without precedent among cytokine-receptor interactions. The IFNAR1-IFN interface is formed by residues of the SD1, SD2, and SD3 subdomains of IFNAR1 and by helices B, C, and D of the IFN molecule

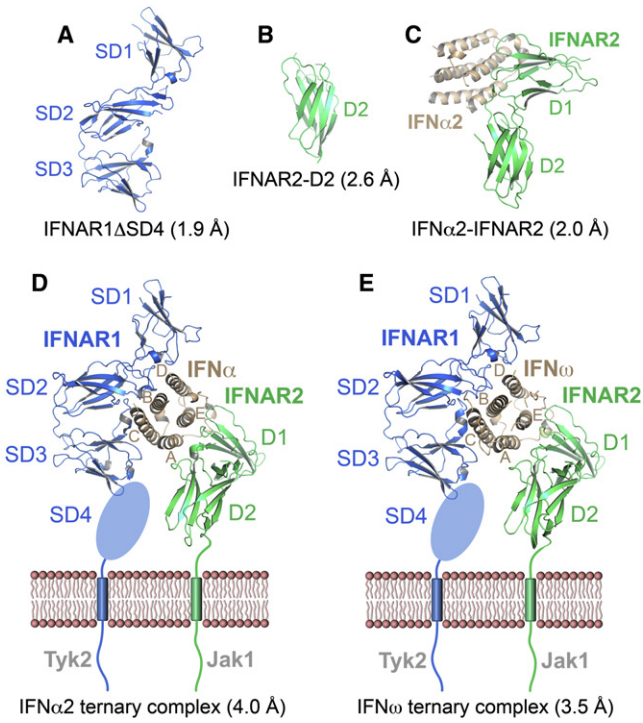

Figure 2. Crystal Structures of Type I IFN Receptor Components and Ligand-Receptor Complexes

Ribbon representations and designated resolutions of (A) IFNAR1ΔSD4; (B) IFNAR2-D2; (C) the IFNα2(HEQ)-IFNAR2 binary complex (IFNα2(HEQ) brown, IFNAR2 green); (D) ternary complex of IFNAR1 (blue), IFNAR2 (green), and IFNα2(YNS); (E) ternary complex of IFNAR1 (blue), IFNAR2 (green), and IFNω. The membrane-proximal SD4 domain of IFNAR1 is depicted as an oval. See also Table S1 and Figure S2.

(Figures 2D and 2E), burying a total surface area of 2197 $Å^2$ (IFNω ternary complex). The IFN ligand primarily binds to IFNAR1 at the level of the hinge between the SD2 and SD3 domains, with the SD1 domain "capping" the top of the IFN molecule. In prior cytokine-receptor complexes of both the type I (e.g., human growth hormone, interleukin-2, erythropoietin, etc.) and type II (e.g., IFNγ, IL-10, etc.) systems, the principal interaction mode is between the cytokine and the loops projecting from the "elbow" formed between two bent Fibronectin-III (FNIII) domains (Figure 3B) (Walter, 2004; Wang et al., 2009). In the case of IFNAR1, the SD2-SD3 tandem FNIII domains appear to be oriented in the opposite direction, such that the loops at the extreme top and bottom ends of the FNIII domains form the major contacts with the IFN ligands in a manner reminiscent of pinchers, whereas the elbow loops that normally bind to cytokines face outward into solvent. The SD1-SD2 tandem FNIII module engages the ligands in a manner that is more representative of a canonical cytokine-binding mode where the elbow contacts the ligand. As the SD1-SD2 and SD3-SD4 modules of IFNAR1 most likely arose by gene duplication, the relative orientation of the domains within the modules is thought to be similar, allowing us to model a position for SD4 (Figure S3A). However, its flexibility implies that there is interdomain variability in its position on a cell surface.

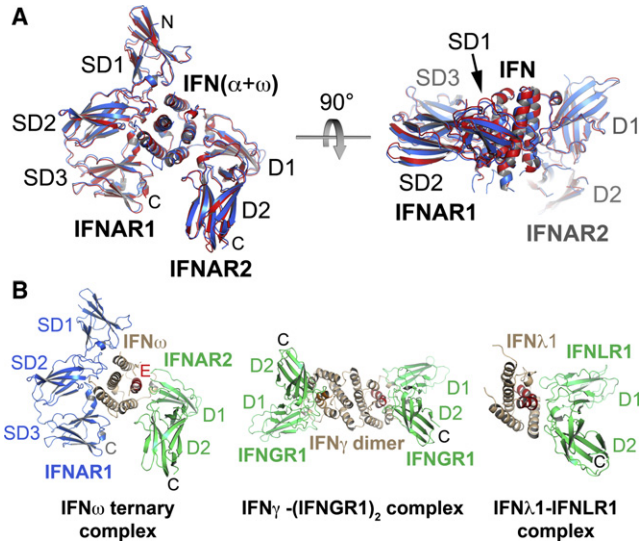

Figure 3. Similar Architectures of Type I IFN Complexes Are Distinct from Type II and Type III IFN Receptor Complexes

(A) The IFN molecules of the IFNω and IFNα2(YNS) ternary complexes were superimposed and are shown in side view and top view. The rmsd for the overall superposition of both structures is 0.9 Å.

(B) The IFNω ternary complex is shown side-by-side with the IFNγ-$(IFNGR1)_2$ complex (PDB accession code: 1FG9) and the IFNλ-IFNLR1 complex (PDB accession code: 3OG6).

N, C: amino and carboxyl termini. SD1–SD3: subdomains of IFNAR1; D1, D2: N- and C-terminal domains of IFNAR2. See also Figure S3B.

On the opposing side of the ligand, both IFNAR2-IFN interfaces are formed between parts of helices A, E, and the A-B loop of the ligand and the IFNAR2-D1 domain and the loop between strands 13/14 in the D2 domain, burying ~1841 $Å^2$ (IFNα2 binary complex) of surface area (Figures 2D and 2E and Figure 4). On IFNAR2, the IFN ligand does not bind at the apex of the elbow region between the D1 and D2 domains of IFNAR2 as seen in most type I and II cytokine-receptor complexes (Figure 3B), but rather almost all of the contact is with the receptor D1 domain. In the ternary complexes, the long axis of the IFN helical bundle is oriented perpendicularly to IFNAR1 but almost parallel to the beta sheets of the IFNAR2 D1 domain. The overall docking position of the ligands bound to IFNAR2 has global similarities to the manner in which the IFNγ dimer engages IFNGR1 (Walter et al., 1995) and also to the IFNλ-IFNLR1 complex (Figure 3B) (Miknis et al., 2010). However, there are large differences in the relative receptor-IFN binding orientations between the different IFN types that clearly distinguish their recognition modes (Figure S3B). The rigid body ligand-binding topology to IFNAR2 is approximately similar to a docking model derived using constraints from NMR and mutagenesis (Nudelman et al., 2010).

Mechanism of IFN Cross-reactivity versus Discrimination by IFNAR2

We compared the ligand-IFNAR2 interfaces from the binary IFNα2-IFNAR2 complex (2.0 Å resolution) (Figures 4A–4D and Figure S2) and the IFNω ternary complex (3.5 Å resolution)

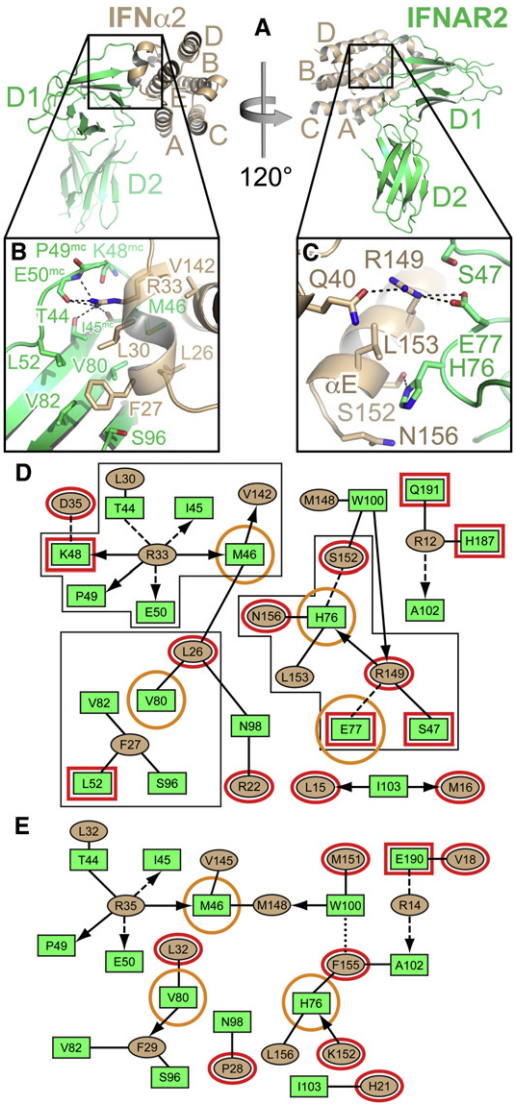

Figure 4. Specificity and Cross-reactivity Determinants between IFN-IFNAR2

(A) Two different views of the IFNα2-IFNAR2 binary complex. Helices of IFNα2 are labeled A–E.

(B) Hotspot residues $Leu30^{\alpha 2}$ and $Arg33^{\alpha 2}$ of IFNα2 and their environment in the interface with IFNAR2. Hydrogen bonds are shown as dashed lines.

(C) Close-up view of $Arg149^{IFN}$, $Glu77^{R2}$, and $His76^{R2}$ and their environment. Hydrogen bonds and salt bridges are depicted as dashed lines.

(D) Two-dimensional interaction map of the IFNα2-IFNAR2 interface. Amino acids are depicted as nodes in the interaction maps (rectangles: IFNAR2; ellipses: IFN). Interactions between side chains are represented by lines, interactions between side chains and backbone are depicted as arrows pointing toward the backbone. Van der Waals interactions and hydrophobic contacts are shown as solid lines, H-bonds or electrostatic interactions as dashed lines, and aromatic interactions as dotted lines. Residues shown in (B) and (C) are bordered with a black line. Structural differences between the IFNα-IFNAR2 and the IFNω-IFNAR2 interfaces are highlighted in red. IFNAR2 residues that, when mutated, differentially affect IFNα and IFNω binding are encircled in orange.

(E) Two-dimensional interaction map of the IFNω-IFNAR2 interface.

See also Figure S2 and Table S2.

(Figure 4E and Figure S2). We elucidated interactions that are conserved across type I IFNs (i.e., "anchor points") versus those that would be ligand specific (Figure 4 and Figure 6). We also assembled previous alanine scanning data (Kalie et al., 2007; Piehler et al., 2000; Roisman et al., 2001, 2005), together with new site-directed mutations prompted by the structures, in order to reconcile the structures with comprehensive energetic maps of the interfaces (Table S2). Overall, most of the residues involved in the IFNα2-IFNAR2 interaction are also found in the IFNω-IFNAR2 interface of the IFNω ternary complex (Figures 4D and 4E), highlighting that the basis of IFN cross-reactivity is through conservation of interactions rather than through highly divergent binding solutions. For clarity, in the two-dimensional contact maps of Figure 4 and Figure 5, *ligand-specific* receptor contacts are circled in red, whereas those with divergent mutational consequences are circled in orange (Table S2). (Note: due to nonidentical sequence lengths [Figure 6G], the numbering of analogous IFNα2 and IFNω residues will often differ by one to three residues throughout the paper.) For example, Arg33$^{\alpha 2}$ (i.e., Arg35 in IFNω), which is conserved in IFNα, IFNω, IFNβ, and IFNε (asparagine in IFNκ), appears to be the single most important residue for the interaction of both IFN ligands with IFNAR2 (Table S2; Figures 4B and 4D). It forms an extensive hydrogen-bonding network with the main chain carbonyl oxygen atoms of Ile45^{R2} and Glu50^{R2} and the side chain of Thr44^{R2}. Replacing Arg33$^{\alpha 2}$ in IFNα2 by alanine destabilizes binding more than any other mutation in IFNα2 (Table S2). Two hydrophobic interaction clusters are present in the IFNα-IFNAR2 interface: the first one is formed between Leu15$^{\alpha 2}$ and Met16$^{\alpha 2}$ of the IFN molecule and Trp100^{R2} and Ile103^{R2} of IFNAR2; the second one comprises Leu26$^{\alpha 2}$, Phe27$^{\alpha 2}$, Leu30$^{\alpha 2}$, and Val142$^{\alpha 2}$ of the ligand and Met46^{R2}, Leu52^{R2}, Val80^{R2}, and Thr44^{R2} of the receptor. Of these, Trp100^{R2}, Ile103^{R2}, Met46^{R2}, Val80^{R2}, Thr44^{R2}, and the ligand residues corresponding to Met148$^{\alpha 2}$, Phe27$^{\alpha 2}$, Leu30$^{\alpha 2}$, and Val142$^{\alpha 2}$ are also involved in the IFNω-IFNAR2 interface. Substituting Met148$^{\alpha 2}$ in IFNα2 or Ile103^{R2} of IFNAR2 results in 10- to 30-fold decreases in binding. As another example, Leu30$^{\alpha 2}$ is conserved in all human IFNs and equates to Leu32$^{\omega}$. Both are involved in similar hydrophobic clusters in IFNAR2 interactions that are also energetically similar (Table S2). Thus, these are energetically critical, shared anchor points mediating IFN cross-reactivity.

In contrast, the mechanism of ligand *discrimination* appears to derive in large part from differential energetics of shared contact positions among the different IFNs. A major ligand-specific difference between the IFNα and IFNω interfaces is related to Arg149$^{\alpha 2}$ in IFNα2, and the analogous Lys152^{IFN} in IFNω, and their respective interaction chemistries with Glu77^{R2}. In the IFNα2-IFNAR2 interface, these two residues (R149A$^{\alpha 2}$ and Glu77^{R2}) stabilize the interaction by forming a salt bridge (Figures 4C and 4D) that is worth about 1.9 kcal/mol in free energy (Figure S4). Substituting Arg149$^{\alpha 2}$ by alanine reduces the affinity between IFNα2 and IFNAR2 by two orders of magnitude (Table S2). Arginine at position 149 is the consensus in all type I IFNs except IFNω, where it is replaced by Lys152$^{\omega}$, that forms an intramolecular salt bridge with Glu149$^{\omega}$ and is within close proximity but is not directly contacting Glu77^{R2} of the receptor. The differential contribution of Glu77^{R2} to the two

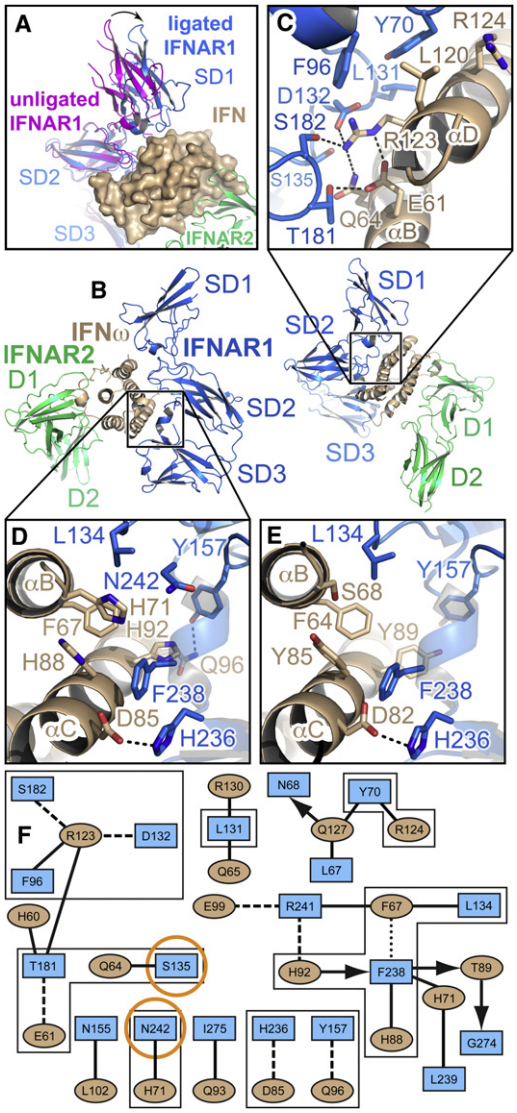

Figure 5. Ligand-Induced Domain Movement in IFNAR1 and the IFN-IFNAR1 Interfaces

(A) Domain movement in IFNAR1 upon IFN binding. Unliganded IFNAR1ΔSD4 (magenta) was superimposed onto subdomains 2 (SD2) and 3 (SD3) of IFNAR1 (blue) in the IFNω ternary complex. The difference in the position of the SD1 domain is depicted as an arrow. The ligand, IFNω, is shown with its molecular surface. See also Figure S3 and http://proteopedia.org/w/Journal:Cell:1.

(B) Two different views of the IFNω ternary complex. SD1–SD3: subdomains of IFNAR1; D1 and D2: subdomains of IFNAR2.

(C) Environment of the hotspot residues Tyr70^{R1} and Arg123$^{\omega}$ in the IFNAR1-IFNω interface. Dashed lines symbolize hydrogen bonds and salt bridges.

(D) Hydrophobic and aromatic interactions between Leu134^{R1} and the hotspot residue Phe238^{R1} in IFNAR1 and Phe67 in IFNω.

(E) The same region as in (D) in the IFNα2-IFNAR1 interface. Hydrogen bonds in the close-up views are depicted as dashed lines.

(F) Interaction map of the IFNω-IFNAR1 interface in the IFNω ternary complex. Amino acids are depicted as nodes in the interaction map (rectangles: IFNAR1; ellipses: IFNω) as used in Figure 4. Residues shown in (C), (D), and (E) are bordered with a black line. IFNAR1 residues that, when mutated, differentially affect IFNα and IFNω binding are encircled in orange.

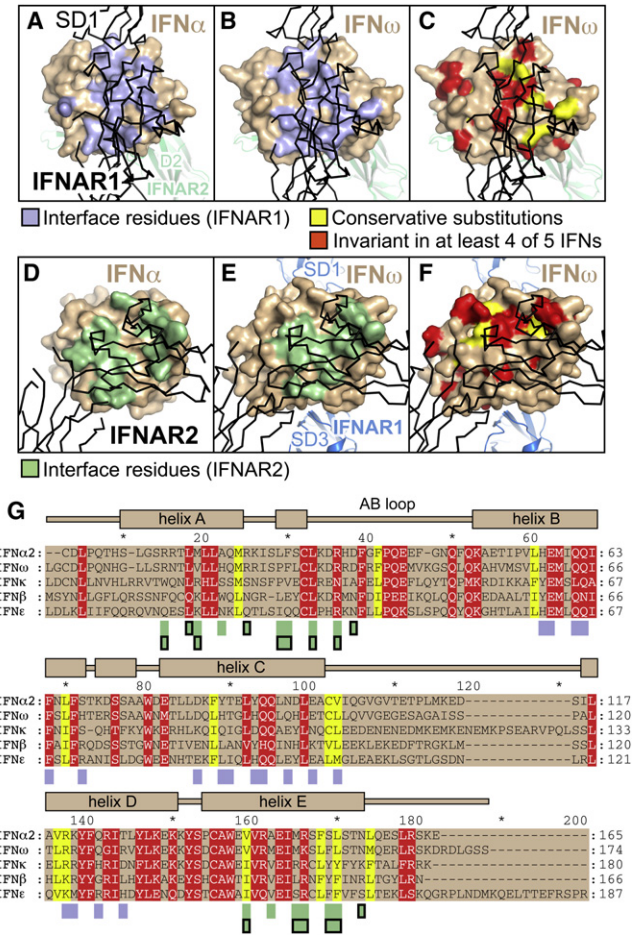

Figure 6. Conservation of Residues in the Ligand-Receptor Interfaces

(A–F) Residues on the surface of IFNω and IFNα involved in the interaction with IFNAR1 (panel A: IFNα ternary complex, panel B: IFNω ternary complex) and IFNAR2 (panel D: IFNα binary complex, panel E: IFNω ternary complex) are colored light blue and green, respectively. Surface residues on IFNω conserved between IFNs are shown in (C) and (F). Physicochemically conserved amino acids are colored yellow; residues that are invariant in at least four of five IFNs (IFNα2, IFNβ, IFNε, IFNκ, and IFNω) are shown in red.

(G) Sequence alignment of human IFNs. Conserved and invariant residues are colored as in (C) and (F). Interacting residues are denoted by rectangles below the alignment, colored according to (A), (B), (D), and (E). Rectangles outlined in black mark interacting residues in the IFNα2 binary complex. The secondary structural elements of IFNω are depicted on top of the alignment.

interfaces is reflected in the observation that its mutation to alanine differentially affects IFNα and IFNω binding: The IFNAR2(E77A) mutant binds IFNα2 with 60-fold lower affinity, whereas the affinity toward IFNω is reduced only 10-fold (Table S2, highlighted in orange). To mimic the connectivity of the IFNα2-binding interface, we made the Lys152Arg$^{\omega}$ swapping mutation (in addition to K152A), which *increases* omega binding by 5-fold (Table S2). To establish the connectivity of Arg at position 152 in IFNω with Glu77^{R2}, we performed double-mutant cycle analyses between E77^{R2} and K152A$^{\omega}$ and K152R$^{\omega}$ (Figure S4). Lysine152$^{\omega}$ binds Glu77^{R2} with a $\Delta\Delta G_{int}$ of 1.3 kcal/mol, whereas Arg in position 152 binds with a $\Delta\Delta G_{int}$ of 2.2 kcal/mol, clearly establishing that, indeed, the consensus arginine at this position is able to form a significantly stronger interaction, supporting the respective structural organization observed for the two different complexes. That the K152R substitution increases binding in IFNω indicates that this position is a critical modular hotspot for ligand discrimination and signaling (discussed below).

There are additional examples of IFN sequence differences, observed as receptor contacts in the structures, playing a role in ligand subtype discrimination. Leu26$^{\alpha 2}$ in IFNα2 equates to Pro28$^{\omega}$ in IFNω (Figures 4D and 4E). The IFNω mutation P28A$^{\omega}$ had no effect on receptor binding, whereas swapping Pro28$^{\omega}$ with Leu26$^{\alpha 2}$ (i.e., P28L$^{\omega}$) reduced binding 6-fold in IFNω. Thus, these residues have evolved distinct energetic values by substituting side chains. Another notable IFNAR2 contacting residue that differs between alpha and omega (Table S2) is Ala145$^{\alpha 2}$, which is Met148 in IFNω. In alpha IFNs, alanine is the consensus residue in position 145 (148 in ω). Yet, M148A$^{\omega}$ reduces binding by ~2.5-fold. The complementary mutation of Ala145 to Met in IFNα2 reduces binding by ~6-fold. This shows a distinct IFN-specific residue preference, and that this position is not simply degenerate for apolar side chains. The subtle apolar volume differences are keenly sensed in ligand discrimination. On the receptor side, Val80^{R2} differentially affects IFNω versus IFNα2 binding (Figures 4B, 4D, and 4E and Table S2, highlighted in orange). Two other residues in IFNAR2, His76^{R2} and Met46^{R2}, also contribute to ligand discrimination (Table S2, highlighted in orange).

IFNAR1 Forms a Diffuse and Broad Interface with the IFN Ligand

The IFNω and IFNα2(YNS) complexes are essentially identical in their binding footprints to IFNAR1 (Figure 3A and Figure 5). We focus on the higher-resolution IFNω ternary complex for a detailed description of the IFN-IFNAR1 interfaces (Figure S2). When the unliganded IFNAR1ΔSD4 structure and IFNAR1 of the ternary complexes are superimposed, it is apparent that the N-terminal SD1 domain and the SD2-SD3 portion of IFNAR1 move relative to each other upon IFN binding (Figure 5A and Figures S3C and S3D), allowing all three subdomains of IFNAR1 to contact the ligand. With the SD2-SD3 domains overlaid and fixed, the conformational change upon complex formation is a quasi-rigid body movement of the SD1 domain by about 10 Å down toward the ligand, bringing Asn68^{R1}, Tyr70^{R1}, and Phe96^{R1} in contact with helix D of the IFN ligand (Figures 5A and 5C). The aromatic rings of Tyr70^{R1} and Phe96^{R1}, together with the side chain of Leu131^{R1} in a loop of the SD2 domain, form a hydrophobic patch that packs against the ligand (Figures 5C and 5F). Arg123$^{\omega}$ on helix D of IFNω forms a critical lynchpin for the SD1-SD2 interaction: it hydrogen bonds to Ser182^{R1} in the SD2 domain, contacts Thr181^{R1} and Phe96^{R1}, and is engaged in a salt bridge with Asp132^{R1} (Figures 5C and 5F). Arg123$^{\omega}$ is intramolecularly stabilized by Glu61$^{\omega}$ that also forms a hydrogen bond with Thr181^{R1}. In addition, the IFNω-IFNAR1 interface is characterized by van der Waals and hydrophobic interactions between Leu134^{R1} (SD2), Phe238^{R1} (SD3), and Phe67$^{\omega}$ in helix B (Figures 5D and 5F). The interactions between

Leu134^{R1}, Phe238^{R1}, and the phenylalanine in the ligand (Phe64$^{\alpha2}$ in IFNα) are conserved in the IFNα-IFNAR1 interface (Figure 5E). Moreover, the contact between His236^{R1} and an aspartate in the ligand is common to the interfaces of both IFNs (Figures 5D and 5E).

It has been demonstrated that the three N-terminal FNIII domains of IFNAR1 (SD1–SD3) are necessary and sufficient for ligand binding (Lamken et al., 2005). In particular, the SD1 segment spanning residues 62–70 is crucial for ligand binding and biological activity, with Val69^{R1} and Tyr70^{R1} as key residues (Cajean-Feroldi et al., 2004). Their role is revealed by our ternary complex structures: Tyr70^{R1} directly contacts the ligand (Figures 5C and 5F), whereas the preceding Val69^{R1} stabilizes the S3-S4 loop. Tyr70^{R1} and F238^{R1} are the only hotspot residues in the ligand-binding site of IFNAR1 (Table S2), highlighting its comparatively energetically flat binding surface compared to IFNAR2. Substituting these residues by alanine reduces the affinity to all tested IFN ligands by more than 10-fold (Table S2).

Most interactions of the IFNω-IFNAR1 interface are conserved in the IFNα2-IFNAR1 interface (Figures 5D and 5E and Figures 6C and 6G). Differences include an aromatic interaction between Tyr157^{R1} of the receptor and Tyr89$^{\alpha2}$ of IFNα2. In IFNω, Tyr157^{R1} hydrogen bonds to Gln96$^{\omega}$ (Figures 5D and 5E). Furthermore, Tyr85$^{\alpha2}$ and Tyr89$^{\alpha2}$ participate in the hydrophobic interaction with Leu134^{R1} and Phe238^{R1} of IFNAR1 and Phe64$^{\alpha2}$ of the ligand (Figure 5E); His71$^{\omega}$, which is contacting Asn242^{R1} in the IFNω complex, is replaced with a serine in IFNα2. The different chemical environments of Asn242^{R1} in the two complexes might contribute to ligand specificity (Table S2, highlighted in orange).

IFNs Are Discriminated through Ligand-Specific Substitutions

In order to analyze the cross-reactivity of the type I IFN receptor, we mapped the interface contact residues and the residues conserved between IFNα2, IFNω, IFNβ, IFNε, and IFNκ onto the surface of the IFN molecules in the ternary complexes (Figure 6). A comparison of the maps of contact residues with the degree of sequence conservation reveals that IFNAR1 and IFNAR2 cross-react with different IFNs by using a few conserved residues on their ligands as anchor points against a background of less- or nonconserved amino acids (Figures 6C, 6F, and 6G). As our mutational analysis has shown, ligand discrimination occurs primarily through distinct energetics of common contacts but also through small numbers of IFN subtype- or sequence-specific contacts. The invariant and conserved ligand residues comprise Leu32$^{\omega}$, Arg35$^{\omega}$, Val145$^{\omega}$, Arg147$^{\omega}$, Glu149$^{\omega}$, Lys152$^{\omega}$, and Leu156$^{\omega}$ in the IFNAR2 interface and His60$^{\omega}$, Glu61$^{\omega}$, Gln64$^{\omega}$, Gln65$^{\omega}$, Phe67$^{\omega}$, Gln93$^{\omega}$, Gln96$^{\omega}$, Leu102$^{\omega}$, Leu120$^{\omega}$, and Arg123$^{\omega}$ in the IFNAR1 interface (residues and numbering referring to IFNω). Of the invariant and conserved IFN residues that form direct contacts with the receptor chains, Leu32$^{\omega}$, Arg35$^{\omega}$, Leu156$^{\omega}$, His60$^{\omega}$, Glu61$^{\omega}$, Gln64$^{\omega}$, Phe67$^{\omega}$, and Arg123$^{\omega}$ influence the energetics of the ligand-receptor interaction, indicated by mutational studies of the corresponding residues in IFNα2 (Leu30$^{\alpha2}$, Arg33$^{\alpha2}$, Leu153$^{\alpha2}$, His57$^{\alpha2}$, Glu58$^{\alpha2}$, Gln61$^{\alpha2}$, Phe64$^{\alpha2}$, and Arg120$^{\alpha2}$; see Table S2).

Probing Differential IFN Signaling with Structure-Based Mutational Analysis

We analyzed two types of IFN mutations for their effects on signaling and function. We chose residues that differ in identity between IFNα2 and IFNω and either directly make energetically important receptor contacts in the structures or are in close proximity to residues that do. The first group includes Ala mutations of these residues (L26A$^{\alpha2}$/P28A$^{\omega}$, L30A$^{\alpha2}$/L32A$^{\omega}$, A145G$^{\alpha2}$/M148A$^{\omega}$, R149A$^{\alpha2}$/K152A$^{\omega}$), as well as swaps of energetically important "sister" residues that are in corresponding positions (P28L$^{\omega}$, K152R$^{\omega}$). A second group of mutations was designed to change the binding affinity to both receptors simultaneously. These were based on the IFNα2(YNS) variant (increases binding to IFNAR1 by ~60-fold) and include YNS/M148A and YNS/L153A, which reduce binding to IFNAR2 by 30- and 10-fold, respectively (Table S2). Proteins harboring both mutations will have an altered balance between their affinities to IFNAR1 (higher affinity) and IFNAR2 (lower affinity). The mutant-binding affinities are shown in Table S2. This extended set of mutations was then used to assess a range of functional consequences of IFN binding to the IFNAR1-IFNAR2 receptors: (1) antiviral (AV) and antiproliferative (AP) activity (Figure 7 and Figure S5), (2) p-STAT activation with respect to EC_{50}s and their relative ratios in different cell types from whole blood (Figures 8A and 8B and Figure S7), (3) gene expression (*PKR*, *CXCL11*, and *TRAIL*) in WISH cells (Figure 8A and Figure S6), and (4) receptor internalization (Figure 8C).

Antiviral and Antiproliferative Activity

Structure-based mutations that result in loss of binding affinity also lead to a decrease in potency for both AV and AP activities and consequently reduce the functional distinction between IFNs (Figure 7 and Figure S5). These data are in general accord with the stability model—antiviral activity is less affected by a loss in binding affinity than antiproliferative activity. Strikingly, mutations increasing binding affinity, as the ones observed for the mutants IFNα2(YNS) and IFNω(K152R), result in a significant increase of the AP activity, but not AV activity (Figure 7B). Indeed, the IFNω(K152R) gain-of-function mutant shows that a single substitution of the corresponding α2 residue results in IFNω behaving more like IFNα2(YNS). This supports the model that IFN-specific polymorphisms engaged in receptor contacts that energetically mediate complex stability play a major role in modulating IFN-specific functional activities (Figure 7B). These results also imply that intermediate affinities are sufficient to induce a maximal AV response, whereas much higher affinities are required to reach the maximal AP potency—in this respect the AP response is more "tunable" (Levin et al., 2011).

p-STAT Activation

We used phospho-flow cytometry and fluorescent cell barcoding to measure phosphorylation levels of STAT1, 3, 4, and 5 in whole blood samples from two human donors (Figures 8A and 8B and Figure S7). Similar to the AV activity, the EC_{50} values obtained for p-STAT activation proportionally increased for weaker binding mutants, whereas for the high-affinity mutants (IFNα2(YNS) and IFNω(K152R)) the same trend was not observed. Indeed, although IFNα2(YNS) induced slightly stronger STAT activation than IFNα2(WT), these differences were very small relative to their very substantial differences in

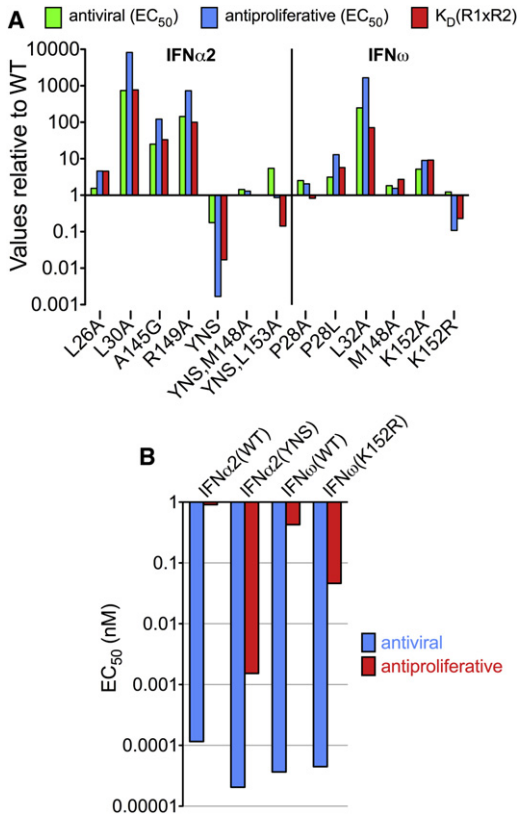

Figure 7. Correlation between Complex Stability and Functional Activity

(A) Antiviral and antiproliferative activity of IFNα2 and IFNω mutants relative to IFNα2(WT) and IFNω(WT), respectively. As a measure of complex stability, the product of the affinities toward IFNAR1 and IFNAR2 was calculated and divided by the value of the respective wild-type protein.

(B) Direct comparison of the antiviral and antiproliferative activity (EC_{50} values) of the high-affinity mutants IFNα2(YNS) and IFNω(K152R) and the corresponding wild-type proteins.

See also Figure S5.

affinity. Similarly, with the IFNω(K152R) mutant, despite its higher binding affinity, this mutant is somewhat less potent in p-STAT activation than IFNω(WT). These results are in accord with the current model that AV activity is well correlated with early p-STAT activation, and AV activity is nearly maximal even for weak binders. In contrast, the extent of STAT activation is not sufficient to explain the potency of the AP response.

p-STAT Ratios

Variable ratios of STAT activation in cell subsets is a striking example of differential signaling through a common receptor by different IFN subtypes (Figure 1F). We analyzed the p-STAT activation ratios induced by the high-affinity IFNα2(YNS) and IFNω(K152R) mutants, as well as the wild-type IFNs, IFNα2 and IFNω, in a mixed population of immune cells, i.e., whole blood samples from humans (Figure 8B and Figure S7). Both mutants followed the same trend in deviations of p-STAT ratios relative to the wild-type IFNs, supporting the idea that by substituting a critical contact residue from one IFN into another, we have narrowed their functional distinction. As the principal effects of these substitutions are on affinity, this further suggests that the stability of the complex is the key determinant for functional distinction of IFNs and also highlights the utility of this metric as a readout of differential signaling activities by IFNs.

Receptor Internalization

We hypothesized that rapid receptor downregulation could be responsible for the nonproportional p-STAT activation observed for IFN mutants with increased binding affinity. Increased IFNAR2 downregulation by an IFNα2 mutant with increased binding affinity toward IFNAR1 has been observed (Jaitin et al., 2006; Marijanovic et al., 2007). Here we show that mutants exhibiting higher binding affinity for IFNAR2 than WT induced a stronger IFNAR2 downregulation (Figure 8C) and faster decrease in p-STAT activation (Figure 8D). The IFNα2(YNS) reduced IFNAR2 by 60%, whereas the $K152R^{\omega}$ mutant almost completely eliminated surface IFNAR2, as opposed to wild-type IFNα2 or IFNω that only reduced the surface IFNAR2 by ~50% (Figure 8C). Thus, increased binding affinities increase the propensity for receptor endocytosis, which leads to faster termination of signaling. The substantially stronger IFNAR2 downregulation exhibited by $K152R^{\omega}$ may explain the surprising increase in EC_{50} of p-STATs seen for this mutant (Figure 8A) due to more rapid (Figure 8C) receptor inactivation in the endosome.

Gene Expression

We asked how receptor-binding affinity regulates the IFN-induced gene expression program. By rtPCR, we measured the levels of *PKR*, *CXCL11*, and *TRAIL* induction following 8 hr of treatment with the different IFN mutants (Figure 8A and Figure S6—note that $P28A^{\omega}$ and $M148A^{\omega}$ were not included in the gene expression analysis). We found a uniform correlation between receptor-binding affinity and gene expression levels. That is, mutants with reduced affinity had a higher EC_{50} for induction of *PKR*, *CXCL11*, and *TRAIL* genes, whereas mutants with higher affinity had a lower EC_{50} for induction of these genes. These data also indicate that the extent of STAT activation as measured by tyrosine phosphorylation does not fully explain the level of gene expression and AP response induced by the different IFN mutants, as in the case of the YNS and $K152R^{\omega}$ mutants. Although YNS is only marginally more potent in activating STATs than IFNα2(WT), it is significantly more potent in inducing *TRAIL*, *PKR*, and *CXCL11* than IFNα2(WT). Interestingly, whereas the EC_{50} for *PKR* gene expression activation is ~50-fold lower for most IFNs than the one measured for *TRAIL* or *CXCL11*, these ratios are significantly smaller (~15-fold) for the three $YNS^{\alpha 2}$ variants and for the $K152R^{\omega}$ mutant (Figure S6), suggesting that tighter-binding IFNs lose some of this differential gene activation, perhaps by sacrificing tunability for affinity.

DISCUSSION

Type I interferons were discovered over 50 years ago as antiviral agents. Subsequent research has shown that the many IFN subtypes show differential activities through common receptor chains. Our studies show that the overall architectures of receptor binding to both IFNα2 and IFNω are nearly identical (Figure 3A), and that the answer to how different IFNs are capable of inducing differential functional effects appears to be ligand discrimination through distinct receptor-binding

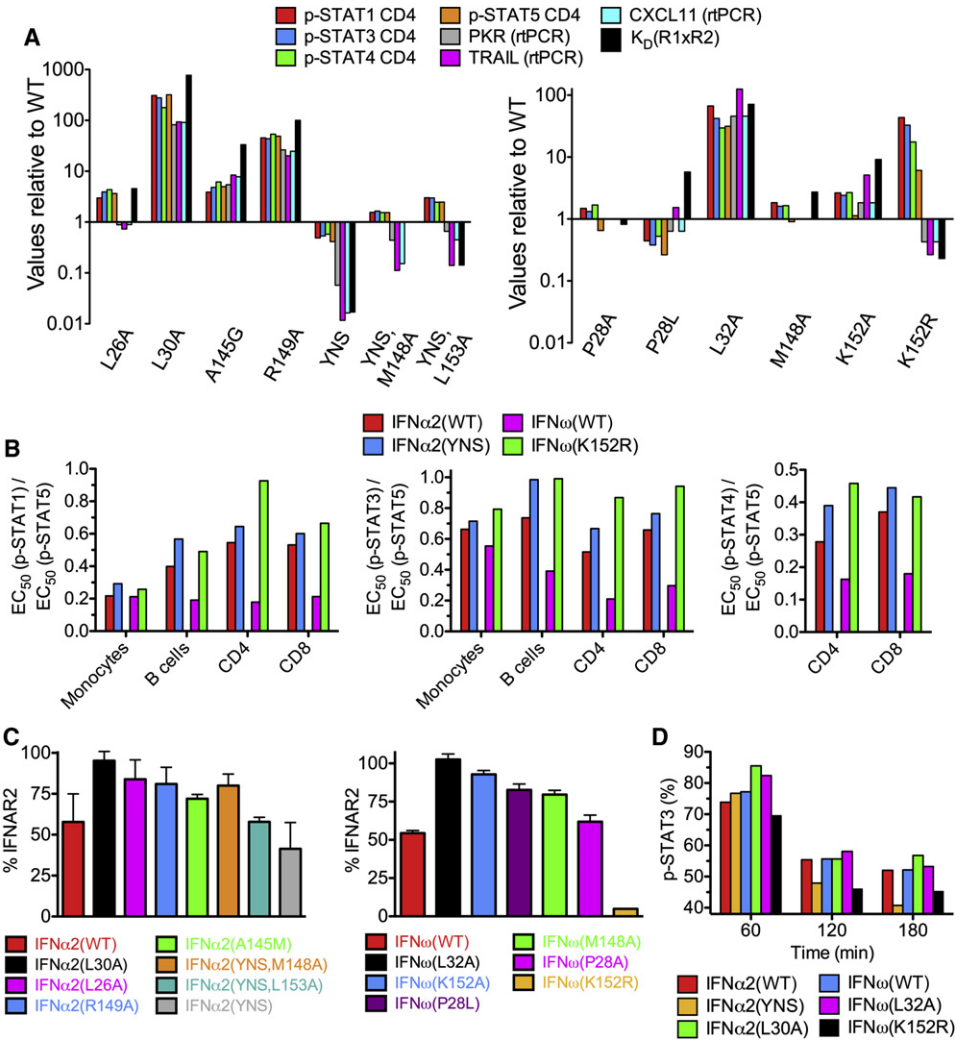

Figure 8. Relationship between STAT Phosphorylation, Gene Expression, and Receptor Downregulation to IFN Mutant-Binding Affinities

(A) Complex stabilities and induction of STAT phosphorylation in CD4 T cells and gene expression (protein kinase R [*PKR*], tumor necrosis factor-related apoptosis-inducing ligand [*TRAIL*], chemokine *CXCL11*) by IFNα2 and IFNω mutants relative to wild-type IFNα2 and IFNω, respectively.

(B) Different EC_{50}(p-STAT) ratios for IFNα2(YNS), IFNω(K152R), IFNα2(WT), and IFNω(WT) in different cell subsets of whole blood from human donors. IFNα2(YNS) and IFNω(K152R) show the same trend of ratio deviations from the wild-type proteins.

(C) Expression levels of IFNAR2 on the surface of B cell lymphoma (Ramos) cells 5 min after stimulation with IFNα2 and IFNω proteins. Shown are mean values with their standard error.

(D) Time course of decrease of p-STAT3 activation induced by different IFNα and IFNω proteins.

See also Figure S6 and Figure S7.

chemistries, which dictate the respective stabilities of the receptor-ligand interactions. The distinct binding chemistries are achieved primarily by differential energetics of shared anchor points and, to a lesser extent, by key amino acid substitutions between IFNs. These ligand-specific differences in the extracellular complex stabilities manifest as perturbations in downstream signaling cascades, in both linear and nonlinear fashions. Mechanistically, different complex stability kinetics could control the relative Jak/Tyk activity toward intracellular substrates of greater or lesser accessibility, which would in turn lead to distinct downstream effector activation profiles and ultimately impact induction of IFN-responsive genes. In this respect, recognition-mediated tuning of differential signaling by the type I IFN receptor system is quite unique for a transmembrane receptor but has parallels to the antigen "proofreading" ability of the T cell receptor to differentially respond to self and foreign peptide-MHC molecules presenting subtly different peptide recognition chemistries.

In the context of prior cytokine receptor structures, IFNAR1 is particularly striking, with participation of three subdomains and a conformational change upon IFN binding (Figure 5A and Figure S3). That this is a bona fide ligand-induced conformational change is corroborated by the importance of the SD1 domain for ligand binding and by FRET measurements suggesting

conformational changes in the ectodomain of IFNAR1 upon IFN binding (Strunk et al., 2008). The conformational change in IFNAR1 is required to form the full spectrum of interactions with the ligand and to allow the formation of a ternary complex that is stable enough to facilitate transphosphorylation between Jak1 and Tyk2. Thus, ligand binding to IFNAR1 will be accompanied by an energetic cost associated with the structural rearrangements required to bring a key hotspot residue into contact and could play a role in tuning responsiveness to different IFN ligands. We suggest that the required conformational change contributes to the reduced binding affinity of IFNAR1 and may result in tighter control of IFN signaling.

In addition to the conformational change, the role of IFNAR1 in ligand responsiveness is also unique compared to IFNAR2. IFNAR1 is not optimized for high binding affinity but rather for functional plasticity. That is, in contrast to the interaction with IFNAR2, binding energy is distributed over a large number of amino acid contacts with relatively low individual contributions and with much lower cooperativity, altogether resulting in lower affinity. For early STAT activation, which is required for the antiviral cellular response, transient ligand interaction with IFNAR1 appears to be advantageous (Moraga et al., 2009). High stability of the ternary complex seems to be more important for a subset of IFN activities requiring prolonged activation of IFN signaling pathways (Coelho et al., 2005; Jaitin et al., 2006). The relatively large binding interface of IFNAR1 for IFN involving three FNIII-like domains provides a versatile means for fine-tuning the binding affinity toward different IFNs and tailoring differential response patterns.

The molecular basis of IFNAR cross-reactivity is unique compared with other shared receptor systems, such as gp130 and common gamma chain (γ_c), and this likely reflects the fact that the IFN interaction chemistry controls signal initiation. gp130 engages different cytokines through entirely distinct binding surfaces that do not appear to share anchor points, whereas γ_c engages in degenerate binding largely through shape complementarity (Wang et al., 2009). What sets the IFNAR system apart is that the IFNAR1/2 heterodimer recognizes and transduces the signal for all 16 IFN subtypes, whereas in the other shared cytokine receptors, signal specificity is determined by different ligand-specific coreceptors heterodimerizing with the shared receptor. In this way, the recognition chemistries of gp130 and γ_c are not important arbiters of signaling specificity.

With regards to function, our mutational and substitution experiments suggest a model whereby ablating or swapping key IFN-specific residues that engage in receptor interactions narrows the functional distinction between IFNs. Importantly, however, the mutational analysis also shows that the local environment of these contacts plays an important role in determining their energetic values in the respective IFN complexes. Mutation of individual positions has complicated energetic consequence. Therefore, ligand-specific residues are not "plug-and-play" in a manner that easily allows one to recapitulate IFN subtype behavior by point mutagenesis. This is to be expected given that the functional distinction of IFN ligands arose, in part, through coevolution of broad receptor-ligand interaction surfaces over hundreds of millions of years. A surprising exception to this was the K152R gain-of-function mutation in IFNω, which, clearly, is a highly modular contact point.

Ligand-specific differences in the stabilities of the complexes are also reflected in variances in the kinetics of receptor downregulation, which terminates signaling. Our studies revealed that increased binding affinities toward IFNAR1 (IFNα2(YNS) mutant) or IFNAR2 (IFNω(K152R) mutant) strongly enhance receptor downregulation, which very likely explains a much more rapid decline in p-STAT activation compared to IFNα2(WT) and IFNω(WT). Increased IFNAR2 downregulation by the higher-affinity IFNβ, compared to IFNα2, has been previously suggested to be responsible for differential cellular responses (Jaitin et al., 2006; Kalie et al., 2007). Here, we have designed an IFN mutant with increased binding affinity toward IFNAR2, which surprisingly induces even stronger downregulation of IFNAR2. Increased IFNAR2 downregulation could explain why the substantially increased binding affinity of these IFN mutants is not accompanied by a significant increase in their AV potency because it is very likely responsible for a rapid decrease in p-STAT levels, as seen after stimulation with IFNα2(YNS) and IFNω(K152R).

In contrast to AV activity, which requires only very low doses of IFN to reach saturation, AP activity benefits from an increased binding affinity (Kalie et al., 2008). Cells need to sense very low levels of IFN and act very fast in order to clear viral infections in their initial stages. On the other hand, antiproliferative activity, which is often linked with apoptosis and tissue damage, needs to be under tighter control to prevent unnecessary damage. These activities will therefore be more tunable over a broad range to changes in the kinetics and strength of the downstream signaling. IFNs, by forming a gradient of complex stabilities, will induce specific profiles of signal activation that will lead to diverse antiproliferative potencies. Taken together, differential IFN signaling activities are mediated by both nonlinear signaling and nonlinear receptor desensitization mechanisms. This type of "ligand proofreading" provides a mechanistic model, now together with a structural framework, for how a common receptor can respond in a graded fashion to different ligands.

EXPERIMENTAL PROCEDURES

Transient Hepatitis C Virus Replication Assay

The transient hepatitis C virus (HCV) replication assay was performed using Huh7.5 cells and a Luciferase reporter system as previously described (Cho et al., 2010). Additional details for this and subsequent experimental procedures can be found in the Extended Experimental Procedures.

Antiproliferative Activity Assay

Antiproliferative assays were performed using WISH cells as described in Moraga et al. (2009).

Protein Expression, Purification, and Complex Formation

The following proteins used in this study were expressed as C-terminally his-tagged constructs from baculovirus using the pAcGp67A vector: human IFNω (including all IFNω mutants), IFNα7, IFNα2(HEQ), IFNAR1ΔSD4 (amino acids 3–305), full-length IFNAR1 ectodomain, IFNAR2 (amino acids 10–205), IFNAR2-D2 (amino acids 104–205). IFNAR2 used in the binary complex was secreted by Hi-5 cells in the presence of Tunicamycin at a concentration of 0.5 mg/l. IFNAR2 (amino acids 7–205) used for IFNω(N80Q) ternary complex formation was expressed using the BacMam expression vector pVL-AD6-L

(Dukkipati et al., 2008) from suspended HEK293 GnTI$^-$ cells grown in Pro293 medium and was deglycosylated with endoglycosidase H_f. Human IFNα2 and all IFNα2 mutants, except HEQ, were expressed in *E. coli* according to published methods (Kalie et al., 2007). Prior to crystallization, all proteins were treated with 3C protease/TEV protease and/or carboxypeptidases A and B to remove C-terminal his-tags. Selenomethionine (SeMet)-labeled proteins from baculovirus were prepared according to a protocol published earlier (Dong et al., 2009).

The IFNω(N80Q) ternary complex was formed by mixing IFNAR1 and IFNω(N80Q) from insect cells with IFNAR2 expressed in HEK293 cells. The IFNα2(YNS) ternary complex was formed by mixing IFNAR1 and IFNAR2 from insect cells and IFNα2(YNS) expressed in *E. coli*. The complexes were formed by mixing individually purified components in approximately stoichiometric ratios; the complexes were purified by gel filtration.

Crystallization and X-Ray Data Collection

All crystallization experiments were carried out using hanging-drop vapor diffusion at 20°C. Individual crystallization conditions can be found in the Extended Experimental Procedures.

Datasets on frozen crystals were collected at beamlines 9.1 (SeMet-IFNAR1ΔSD4), 9.2 (osmium-derivatized IFNAR1ΔSD4; SeMet-IFNAR2-D2), and 11.1 (native dataset of IFNAR1ΔSD4) of the Stanford Synchrotron Radiation Lightsource (SSRL) and at beamlines 8.2.1 (IFNα2(YNS) ternary complex) and 8.2.2 (IFNα2(HEQ)-IFNAR2 binary complex; IFNω(N80Q) ternary complex) of the Advanced Light Source (ALS), Berkeley. All data were indexed, integrated, and scaled with the XDS package (Kabsch, 1993).

Structure Determination and Refinement

Phases for IFNAR1ΔSD4 were obtained by single isomorphous replacement with anomalous scattering (SIRAS) in the program autoSHARP (Vonrhein et al., 2007) using the osmium derivative and the native dataset.

The structure of the SeMet-labeled IFNAR2-D2 domain was determined by single-wavelength anomalous diffraction (SAD) using autoSHARP.

The IFNα2(HEQ)-IFNAR2 binary complex, IFNα2(YNS) ternary complex, and IFNω(N80Q) ternary complex were all solved by molecular replacement with the program Phaser (McCoy et al., 2007). All X-ray structures described were refined with Phenix (Adams et al., 2010). Molecular graphics images were prepared using PyMOL (Schrödinger).

Affinity Measurements

All binding data of IFNs and the ECD of IFNAR2 were determined by surface plasmon resonance on a ProteOn XPR36 machine (BIO-RAD) using purified proteins. Binding of IFNα2(YNS) and IFNω to immobilized IFNAR1 was probed by simultaneous total internal reflection fluorescence spectroscopy (TIRFS) and reflectance interference (RIF) detection.

Phospho-Flow Analysis of Intracellular Signaling

Analysis of intracellular signaling in whole blood was performed as previously described (Krutzik and Nolan, 2006). Briefly, whole blood samples from two donors were warmed to 37°C and stimulated with increasing concentrations of the appropriate cytokine for 30 min. After samples were fixed and lysed, samples were fluorescently barcoded with DyLight 800 and Pacific Orange dyes as previously described. After barcoding and combining, samples were stained for 1 hr with CD3 PE, CD4 Pacific Blue, CD20 PerCP-Cy5.5, CD33 PE-Cy7, and a combination of p-STAT1 Ax647 and p-STAT3 Ax488 or p-STAT5 Ax647 and p-STAT4 Ax488. Analysis was performed on a Becton Dickinson LSRII equipped with 405, 488, and 633 nm lasers. Data analysis was performed in Cytobank software. Log median fluorescence intensity values were plotted against cytokine concentration to yield dose-response curves.

Analysis of IFNAR2 Downregulation

Downregulation experiments were performed using Ramos cells stimulated with IFN proteins for 5 min, followed by anti-IFNAR2 monoclonal antibody (mAb) staining as described in Jaitin et al. (2006) and Marijanovic et al. (2007).

Analysis of STAT Phosphorylation Kinetics

Ramos cells were stimulated with 10 nM of IFN mutants for the indicated times according to the protocol in Marijanovic et al. (2007). Samples were analyzed by phospho-flow cytometry.

Quantitative PCR

Selected human IFN-stimulated gene expression levels were measured with the ABI Prism 7300 Real-Time PCR System using previously described methods (Levin et al., 2011).

ACCESSION NUMBERS

Coordinates and structure factors have been deposited within the Research Collaboratory for Structural Bioinformatics (RCSB) Protein Data Bank (PDB) under accession codes 3S98 (IFNAR1ΔSD4), 3S8W (IFNAR2-D2), 3S9D (binary IFNα-IFNAR2 complex), 3SE4 (ternary IFNω complex), and 3SE3 (ternary IFNα complex).

SUPPLEMENTAL INFORMATION

Supplemental Information includes Extended Experimental Procedures, seven figures, and two tables and can be found with this article online at doi:10.1016/j.cell.2011.06.048.

ACKNOWLEDGMENTS

We thank Natalia Goriatcheva for expert technical assistance, the staff at SSRL and ALS for their assistance, and David Canner for preparing the Proteopedia pages. K.C.G. is an Investigator of the Howard Hughes Medical Institute. This work was also supported by NIH-RO1-AI51321 (K.C.G.) and NIH-RO1-AI087917 (J.S.G.), C.T. is supported by a long-term postdoctoral fellowship of the International Human Frontier Science Program Organization. G.S. and J.P. are supported by the European Community's FP7/2007-2013 under GA no. 223608 (IFNaction).

Received: February 3, 2011
Revised: May 17, 2011
Accepted: June 15, 2011
Published: August 18, 2011

REFERENCES

Adams, P.D., Afonine, P.V., Bunkóczi, G., Chen, V.B., Davis, I.W., Echols, N., Headd, J.J., Hung, L.W., Kapral, G.J., Grosse-Kunstleve, R.W., et al. (2010). PHENIX: a comprehensive Python-based system for macromolecular structure solution. Acta Crystallogr. D Biol. Crystallogr. *66*, 213–221.

Bleicher, L., de Moura, P.R., Watanabe, L., Colau, D., Dumoutier, L., Renauld, J.C., and Polikarpov, I. (2008). Crystal structure of the IL-22/IL-22R1 complex and its implications for the IL-22 signaling mechanism. FEBS Lett. *582*, 2985–2992.

Bogdan, C. (2000). The function of type I interferons in antimicrobial immunity. Curr. Opin. Immunol. *12*, 419–424.

Borden, E.C., Sen, G.C., Uze, G., Silverman, R.H., Ransohoff, R.M., Foster, G.R., and Stark, G.R. (2007). Interferons at age 50: past, current and future impact on biomedicine. Nat. Rev. Drug Discov. *6*, 975–990.

Cajean-Feroldi, C., Nosal, F., Nardeux, P.C., Gallet, X., Guymarho, J., Baychelier, F., Sempé, P., Tovey, M.G., Escary, J.L., and Eid, P. (2004). Identification of residues of the IFNAR1 chain of the type I human interferon receptor critical for ligand binding and biological activity. Biochemistry *43*, 12498–12512.

Chill, J.H., Quadt, S.R., Levy, R., Schreiber, G., and Anglister, J. (2003). The human type I interferon receptor: NMR structure reveals the molecular basis of ligand binding. Structure *11*, 791–802.

Cho, N.J., Dvory-Sobol, H., Lee, C., Cho, S.J., Bryson, P., Masek, M., Elazar, M., Frank, C.W., and Glenn, J.S. (2010). Identification of a class of HCV

inhibitors directed against the nonstructural protein NS4B. Sci. Transl. Med. *2*, 15ra16.

Coelho, L.F., Magno de Freitas Almeida, G., Mennechet, F.J., Blangy, A., and Uzé, G. (2005). Interferon-alpha and -beta differentially regulate osteoclastogenesis: role of differential induction of chemokine CXCL11 expression. Proc. Natl. Acad. Sci. USA *102*, 11917–11922.

Dong, G., Wearsch, P.A., Peaper, D.R., Cresswell, P., and Reinisch, K.M. (2009). Insights into MHC class I peptide loading from the structure of the tapasin-ERp57 thiol oxidoreductase heterodimer. Immunity *30*, 21–32.

Dukkipati, A., Park, H.H., Waghray, D., Fischer, S., and Garcia, K.C. (2008). BacMam system for high-level expression of recombinant soluble and membrane glycoproteins for structural studies. Protein Expr. Purif. *62*, 160–170.

Gaboriaud, C., Uzé, G., Lutfalla, G., and Mogensen, K. (1990). Hydrophobic cluster analysis reveals duplication in the external structure of human alpha-interferon receptor and homology with gamma-interferon receptor external domain. FEBS Lett. *269*, 1–3.

García-Sastre, A., and Biron, C.A. (2006). Type 1 interferons and the virus-host relationship: a lesson in détente. Science *312*, 879–882.

Horton, H.M., Hernandez, P., Parker, S.E., and Barnhart, K.M. (1999). Antitumor effects of interferon-omega: in vivo therapy of human tumor xenografts in nude mice. Cancer Res. *59*, 4064–4068.

Isaacs, A., and Lindenmann, J. (1957). Virus interference. I. The interferon. Proc. R. Soc. Lond. B Biol. Sci. *147*, 258–267.

Jaitin, D.A., Roisman, L.C., Jaks, E., Gavutis, M., Piehler, J., Van der Heyden, J., Uze, G., and Schreiber, G. (2006). Inquiring into the differential action of interferons (IFNs): an IFN-alpha2 mutant with enhanced affinity to IFNAR1 is functionally similar to IFN-beta. Mol. Cell. Biol. *26*, 1888–1897.

Jaks, E., Gavutis, M., Uzé, G., Martal, J., and Piehler, J. (2007). Differential receptor subunit affinities of type I interferons govern differential signal activation. J. Mol. Biol. *366*, 525–539.

Jones, B.C., Logsdon, N.J., and Walter, M.R. (2008). Structure of IL-22 bound to its high-affinity IL-22R1 chain. Structure *16*, 1333–1344.

Josephson, K., Logsdon, N.J., and Walter, M.R. (2001). Crystal structure of the IL-10/IL-10R1 complex reveals a shared receptor binding site. Immunity *15*, 35–46.

Kabsch, W. (1993). Automatic processing of rotation diffraction data from crystals of initially unknown symmetry and cell constants. J. Appl. Cryst. *26*, 795–800.

Kalie, E., Jaitin, D.A., Abramovich, R., and Schreiber, G. (2007). An interferon alpha2 mutant optimized by phage display for IFNAR1 binding confers specifically enhanced antitumor activities. J. Biol. Chem. *282*, 11602–11611.

Kalie, E., Jaitin, D.A., Podoplelova, Y., Piehler, J., and Schreiber, G. (2008). The stability of the ternary interferon-receptor complex rather than the affinity to the individual subunits dictates differential biological activities. J. Biol. Chem. *283*, 32925–32936.

Krutzik, P.O., and Nolan, G.P. (2006). Fluorescent cell barcoding in flow cytometry allows high-throughput drug screening and signaling profiling. Nat. Methods *3*, 361–368.

Lamken, P., Gavutis, M., Peters, I., Van der Heyden, J., Uzé, G., and Piehler, J. (2005). Functional cartography of the ectodomain of the type I interferon receptor subunit ifnar1. J. Mol. Biol. *350*, 476–488.

Levin, D., Harari, D., and Schreiber, G. (2011). Stochastic receptor expression determines cell fate upon interferon treatment. Mol. Cell. Biol. Published online June 21 2011. 10.1128/MCB.05251-11.

Li, Z., Strunk, J.J., Lamken, P., Piehler, J., and Walz, T. (2008). The EM structure of a type I interferon-receptor complex reveals a novel mechanism for cytokine signaling. J. Mol. Biol. *377*, 715–724.

Marijanovic, Z., Ragimbeau, J., van der Heyden, J., Uzé, G., and Pellegrini, S. (2007). Comparable potency of IFNalpha2 and IFNbeta on immediate JAK/STAT activation but differential down-regulation of IFNAR2. Biochem. J. *407*, 141–151.

McCoy, A.J., Grosse-Kunstleve, R.W., Adams, P.D., Winn, M.D., Storoni, L.C., and Read, R.J. (2007). Phaser crystallographic software. J. Appl. Cryst. *40*, 658–674.

Miknis, Z.J., Magracheva, E., Li, W., Zdanov, A., Kotenko, S.V., and Wlodawer, A. (2010). Crystal structure of human interferon-lambda1 in complex with its high-affinity receptor interferon-lambdaR1. J. Mol Biol. *404*, 650–664.

Moraga, I., Harari, D., Schreiber, G., Uzé, G., and Pellegrini, S. (2009). Receptor density is key to the alpha2/beta interferon differential activities. Mol. Cell. Biol. *29*, 4778–4787.

Nudelman, I., Akabayov, S.R., Schnur, E., Biron, Z., Levy, R., Xu, Y., Yang, D., and Anglister, J. (2010). Intermolecular interactions in a 44 kDa interferon-receptor complex detected by asymmetric reverse-protonation and two-dimensional NOESY. Biochemistry *49*, 5117–5133.

Pestka, S., Krause, C.D., and Walter, M.R. (2004). Interferons, interferon-like cytokines, and their receptors. Immunol. Rev. *202*, 8–32.

Piehler, J., Roisman, L.C., and Schreiber, G. (2000). New structural and functional aspects of the type I interferon-receptor interaction revealed by comprehensive mutational analysis of the binding interface. J. Biol. Chem. *275*, 40425–40433.

Quadt-Akabayov, S.R., Chill, J.H., Levy, R., Kessler, N., and Anglister, J. (2006). Determination of the human type I interferon receptor binding site on human interferon-alpha2 by cross saturation and an NMR-based model of the complex. Protein Sci. *15*, 2656–2668.

Radhakrishnan, R., Walter, L.J., Hruza, A., Reichert, P., Trotta, P.P., Nagabhushan, T.L., and Walter, M.R. (1996). Zinc mediated dimer of human interferon-alpha 2b revealed by X-ray crystallography. Structure *4*, 1453–1463.

Roisman, L.C., Piehler, J., Trosset, J.Y., Scheraga, H.A., and Schreiber, G. (2001). Structure of the interferon-receptor complex determined by distance constraints from double-mutant cycles and flexible docking. Proc. Natl. Acad. Sci. USA *98*, 13231–13236.

Roisman, L.C., Jaitin, D.A., Baker, D.P., and Schreiber, G. (2005). Mutational analysis of the IFNAR1 binding site on IFNalpha2 reveals the architecture of a weak ligand-receptor binding-site. J. Mol. Biol. *353*, 271–281.

Schindler, C., and Plumlee, C. (2008). Inteferons pen the JAK-STAT pathway. Semin. Cell Dev. Biol. *19*, 311–318.

Strunk, J.J., Gregor, I., Becker, Y., Li, Z., Gavutis, M., Jaks, E., Lamken, P., Walz, T., Enderlein, J., and Piehler, J. (2008). Ligand binding induces a conformational change in ifnar1 that is propagated to its membrane-proximal domain. J. Mol. Biol. *377*, 725–739.

Uzé, G., Schreiber, G., Piehler, J., and Pellegrini, S. (2007). The receptor of the type I interferon family. Curr. Top. Microbiol. Immunol. *316*, 71–95.

van Boxel-Dezaire, A.H., Rani, M.R., and Stark, G.R. (2006). Complex modulation of cell type-specific signaling in response to type I interferons. Immunity *25*, 361–372.

Vonrhein, C., Blanc, E., Roversi, P., and Bricogne, G. (2007). Automated structure solution with autoSHARP. Methods Mol. Biol. *364*, 215–230.

Walter, M.R. (2004). Structural analysis of IL-10 and Type I interferon family members and their complexes with receptor. Adv. Protein Chem. *68*, 171–223.

Walter, M.R., Windsor, W.T., Nagabhushan, T.L., Lundell, D.J., Lunn, C.A., Zauodny, P.J., and Narula, S.K. (1995). Crystal structure of a complex between interferon-gamma and its soluble high-affinity receptor. Nature *376*, 230–235.

Wang, X., Lupardus, P., Laporte, S.L., and Garcia, K.C. (2009). Structural biology of shared cytokine receptors. Annu. Rev. Immunol. *27*, 29–60.

Zdanov, A. (2010). Structural analysis of cytokines comprising the IL-10 family. Cytokine Growth Factor Rev. *21*, 325–330.